Lidar-observed enhancement of aerosols in UTLS over the Tibetan Plateau during the Asian summer monsoon

Q. S. He[1],C. C. Li[2], J. Z. Ma[3],H. Q. Wang[4], X. L.Yan[3], Z. R. Liang[1],and G. M. Qi[5]

[1]Shanghai Meteorological Service, Shanghai, China

[2]Department of Atmospheric and Oceanic Sciences, School of Physics, Peking University, Beijing, China

[3]Chinese Academy of Meteorological Sciences, Beijing, China

[4]College of Environmental Science and Engineering, Donghua University, Shanghai, China

[5]Germu Meteorological Bureau, Qinghai, China

Correspondence to: C. Li (ccli@pku.edu.cn)

Abstract.

Vertical profiles of aerosol extinction coefficients were measured by an Micro Pulse Lidar at Naqu (31.5 ℃N, 92.1 ℃E, 4508m a.m.s.l.), a meteorological station located on the central part of the Tibetan Plateau during summer 2011. Observations show a persistent maximum in aerosol extinction coefficients in the upper troposphere–lower stratosphere (UTLS). These aerosol layers were generally located at an altitude of 18–19 km a.m.s.l., 1–2 km higher than the tropopause, with broad layer depth ranging approximately 3–4 km and scattering ratio of 4-9. The aerosol layers in UTLS wore off gradually with the reducing intensity of the Asian monsoon over the Tibetan Plateau at the end of August. Aerosols in UTLS over the plateau appear to be influenced by Nabro volcano eruption on 13 June 2011. Variations in these aerosols are also found to be closely related to the intensity of underlying deep convection, indicating that deep convection plays an important role in the accumulation of aerosols in UTLS over the Tibetan Plateau.

1 Introduction

Aerosols in the upper troposphere–lower stratosphere (UTLS) play an important role in the global/regional climate system and the geochemical cycle (Hanson et al.,

1994; Borrmann et al., 1997; Solomon et al., 1997). They also influence atmospheric ozone budgets through providing surface areas for efficient heterogeneous reactions (Keimet al., 1996; Solomon, 1999). Using the Stratospheric Aerosol and Gas Experiment II(SAGE II) data, Li et al. (2001) found that aerosol concentrations near 100 hPa are higher over the Tibetan Plateau than over China's central and northern regions in summer. Recent observations by balloon-borne optical particle counter (Tobo et al.,2007) and aircraft-borne measurements (Keim et al., 1996; Solomon, 1997) showed that soot-containing liquid aerosols with the major components of fine particles may also affect the aerosol layer near the tropopause. Appearance of cold tropopause in the upper troposphere (possibly in the lower stratosphere also) has been considered as an important factor to explain the enhancement of tropopause aerosols observed in summer over the Plateau (Kim et al., 2003). This observational fact is important from the point view of heterogeneous reactions on aerosol surfaces since gas-to-particle conversion processes are generally more active in low temperature. During summer, the elevated surface heating and rising air associated with persistent deep convection over the Tibetan Plateau leads to anticyclonic circulation and divergence in the UTLS(Yanai et al., 1992; Hoskins and Rodwell, 1995; Highwood and Hoskins, 1998), where persistently enhanced pollutants such as aerosols, CO, methane and nitrogen oxides, as well as water vapor, can be linked to the rapid vertical transport of surface air from Asia, India and Indonesia in deep convection and confinement by strong anticyclonic circulation (Rosenlof et al., 1997; Jackson et al., 1998; Dethof et al., 1999; Park et al., 2004; Filipiak et al., 2005; Li et al., 2005a; Fu et al., 2006).

Volcanic eruption, though as occasional event, can inject amounts of ash and sulfur dioxide (SO_2) into the stratosphere, and the injected SO_2 was oxidized to sulfuric acid particles through homogeneous nucleation (Wu et al., 1994). The Nabro stratovolcano in Eritrea, northeastern Africa, erupted on 13 June 2011, injecting approximately 1.3 teragrams of SO_2 to altitudes of 9 to 14 kilometers in the upper troposphere, which resulted in a large aerosol enhancement in the stratosphere(Bourassa et al., 2012). This event has been observed by lidar networks

such as EARLINET, MPLNET and NDACC with independent lidar groups and satellite Cloud–Aerosol Lidar and Infrared Pathfinder Satellite Observations (CALIPSO) to track the evolution of the stratospheric aerosol layer in various parts of the globe (Uchino et al., 2012; Sawamura et al., 2013), and other instruments, such as the Infrared Atmospheric Sounding Interferometer (Clarisse et al., 2013) and the ground-based spectrometry of twilight sky brightness (Tukiainen et al., 2013). Bourassa et al. (2012) found that the aerosol enhancement built while remaining confined for several weeks to the region between central Asia and the Middle East after eruption of Nabro volcano using the limb scanning Optical Spectrograph and Infra-Red Imaging System (OSIRIS) satellite instrument.

The aerosols from Nabro eruption might overlap with the background tropopause aerosols in summer, changing their properties and evolvement in UTLS over the Plateau. A clarification of the mechanisms that aerosols transport into and disperse out of the UTLS over the Plateau is an important step toward understanding tropospheric influences on hydration and chemical composition in the global stratosphere. Knowing the height dependence of the aerosol changes is important for understanding the mechanisms responsible for the transport of aerosols from the troposphere to the stratosphere over the Tibetan Plateau; however, a variety of aerosol vertical distributions and optical properties over the Tibetan Plateau has not been assessed in a satisfactory manner due to lack of continuous direct observations.

The vertical distributions of aerosol extinction coefficients were measured over the Tibetan Plateau in the summer of 2011, as part of the project “Tibetan Ozone, Aerosol and Radiation” (TOAR). In this study, the lidar and radiosonde measurement results are presented and compared with satellite data. We find a persistent maximum in aerosol extinction coefficients in the UTLS within the anticyclone, and show that such aerosol accumulation can be linked to the eruption of Nabro volcano and the development of the Tibetan deep convective systems. These results indicate that volcanic aerosol dispersed with the weakening of Tibetan anticyclonic circulation and deep convection could primarily affect aerosol and hence radiation properties near the tropopause over the Tibetan Plateau.

2 Measurements and Data

2.1 Micro Pulse Lidar

An Micro Pulse Lidar (MPL-4B, Sigma Space Corp., USA) was operated at the Naqu Meteorological Bureau (31.5 °N, 92.1 °E, 4508m a.m.s.l.) on the central part of the Tibetan Plateau. The MPL is a backscatter lidar which uses an Nd:YLF laser with an output power of 12 μJ at 532nm and 2500 Hz repetition rate. The diameter of the receiving telescope is 20 cm, and the field of view is 0.1 mrad. The vertical resolution of the lidar observation is 30m, and the integration time is 30 s. Data obtained on the cloud-free days during nighttime were selected in order to avoid the disturbance of cloud and/or rain to column-averaged lidar ratio and solar noise.

In general, the inversion of the LIDAR profile is based on the solution of the single scattering LIDAR equation:

$$P(r) = O_c(r) CE \frac{\beta(r)}{r^2} \exp[-2\int_0^r \sigma(z)dz] \quad (1)$$

where r is the range, C is the LIDAR constant, which incorporates the transmission and the detection efficiency, and E is the laser pulse energy. $\beta(r)$ represents the total backscattering coefficient $\beta(r)= \beta_m(r)+ \beta_a(r)$, $\sigma(r)$ is the total extinction coefficient $\sigma(r)= \sigma_m(r)+ \sigma_a(r)$, $\beta_a(r)$ and $\sigma_a(r)$ are aerosol backscattering and extinction coefficients, respectively. $\beta_m(r)$ and $\sigma_m(r)$ are molecular contributions to the backscattering and the extinction coefficients, respectively. They can be evaluated by the Rayleigh-scattering theory from the Standard Atmosphere 1976 (NASA, 1976). But here the molecular extinction coefficients are evaluated using temperature and pressure from the radiosondes released at the lidar field site twice a day. $O_c(r)$ is the overlap correction as a function of the range caused by field-of-view conflicts in the transceiver system. Systematic errors of P(r) were mainly observed in the lowest altitudes where an incomplete overlap between the emitted laser beam and the telescope field-of-view can led to an underestimation of aerosol backscatter and extinction coefficients. Since the majority of aerosols are contained in the first several kilometers of the atmosphere, the overlap problem must be solved. Overlap is

typically solved experimentally, using techniques outlined by Campbell et al. (2002). The starting point is an averaged data sample where the system is pointed horizontally with no obscuration. By choosing a time when the atmosphere is well mixed, such as late afternoon, or, even better, when the aerosol loading is low, backscattering through the layer is roughly assumed to be constant with range (i.e., the target layer is assumed to be homogeneous). The similar overlap calibration was carried out at the beginning of this field experiment.

The vertical profile of aerosol extinction coefficient σ_a is determined by a near end approach in solving the lidar equation as proposed by Fernald (1984). Considered the period of TOAR campaign was only two months after eruption of Nabro volcano, volcanic aerosols were still freshly nucleated particles with small size. The lidar ratios should therefore feature rather high (Müller et al., 2007). Sawamura et al. (2013) employed the mean lidar ratio value of 50 sr at 532 nm for most groups of global lidar networks to trace the evolution of the stratospheric aerosol layer from Nabro volcano eruption. Therefore, a column averaged lidar ratio of 50 sr is assumed for all measurement examples in this study.

We identify the boundaries of aerosol layer in the UTLS from the lidar extinction coefficient profiles. The lowest bin with σ_a=0.002 km^{-1} above 18 km is identified as the top of aerosol layer H_t and the bin with minimum value of σ_s between 10 km and 16 km as the layer base H_b. The visible optical depth of the aerosol layer is derived by integrating the values of σ_a between H_b and H_t.

2.2 Radiosonde Observations

During the field campaigns, 76 L-band (GTS1) electronic radiosondes (Nanjing Bridge Machinery Co., Ltd., China) were launched to provide vertical profiles of pressure, temperature, and humidity up to 25 km to 30 km high. The radiosondes were released at the lidar field site in Naqu twice a day at 0000 and 1200 UTC.

Eleven weather balloons with Vaisala RS92 radiosondes (Vömel et al., 2007) have been launched to provide profiles of air temperature, relative humidity RH, wind speed and wind direction usually up to the mid stratosphere. The RH can be measured between 0 and 100% with a resolution of 1% and an accuracy of 5% at -50 ℃

(Miloshevich et al., 2006; Wärhn et al., 2004). While Miloshevich et al. (2009) found that the RH measured by RS92 has a moist bias in the lower stratosphere (LS) and a dry bias in the upper troposphere (UT). The Cryogenic Frostpoint Hygrometer (CFH) is a lightweight (400 g) microprocessor-controlled instrument and operates on the chilled-mirror principle using a cryogenic liquid as cooling agent. It includes several improvements over the similar NOAA/CMD instrument. It is currently designed to be combined with ozone sondes to provide simultaneous profiles of water vapor and ozone(Vömel et al., 2007). CFH has been taken in many inter comparison experiment as an absolute reference for water vapor measurements, including the validation of Aura MLS water vapor products. We compared RS92 RH measurements with simultaneous water vapor measurements from CFH on 13 August 2011. After applying the time-lag and solar radiation bias corrections, corrected RS92 RH measurements show agreement with CFH in the troposphere. The mean difference between corrected RS92 RH measurements and CFH is a dry bias of 2.9% in the ground layer, while the mean differences in 5-10 km, 10-15 km and tropopause transition layer region are 1%, 0.6% and 1.4% moist bias, respectively. Therefore, the accuracy of corrected RS92 RH measurements is comparable to the accuracy of CFH in the UTLS (Yan, 2012).

2.3 Satellite Observations

The Cloud–Aerosol Lidar with Orthogonal Polarization (CALIOP) onboard CALIPSO (Winker et al.,2003), is used to characterize aerosol extinction profiles in the UTLS, which is a three-channel (532 nm parallel, 532 nm perpendicular, 1064 nm) elastic lidar receiving light at the same wavelength as the emitted laser frequency. CALIOP sends short and intense pulses (1064 and 532 nm) of linearly polarized laser light downward towards the Earth. The atmospheric backscatter profile is retrieved at 60 m vertical resolution from 8–20 km with a horizontal resolution of 1 km. The Level 2 aerosol extinctions at 532nm of CALIOP (version 3.0) were used to compared with the ground based MPL on the Plateau, which can be obtained at http://www-calipso.larc.nasa.gov/tools/data_avail/. CALIOP data are selected over a 300 km x 300 km square with a MPL location in its center.

National Oceanic and Atmospheric Administration (NOAA) satellites provide an outgoing longwave radiation (OLR) product for the top of the atmosphere. OLR data are calculated on a daily basis by the Climate Diagnostic Center (CDC), a division of NOAA (Liebmann and Smith 1996). The horizontal resolution is 2.5° by 2.5°. Missing values are computed by applying spatial and temporal interpolations. The OLR in this data set is calculated by converting 10 μm to 12 μm channel radiances measured by the Advanced High Resolution Radiometer aboard the NOAA operational polar orbiting satellites. The daily mean is the average of one daytime and one nighttime measurement. The OLR emitted by high, cold, deep convective clouds is much lower than that by warm low clouds or by the Earth's surface. Usually, values of less than 200 W m^{-2} indicate deep convection (Fujiwara et al., 2009). Deep convection, in turn, indicates the regions with extensive lifting of air that may act as source regions for aerosol layer.

We used the water vapor profiles observations (version 3.3) from the Microwave Limb Sounder (MLS) on the NASA Aura satellite (Waters et al., 2006). Aura MLS measurements include water vapor, ozone and carbon monoxide that are useful tracers of tropospheric and stratospheric air; these data have been used to document enhanced levels of carbon monoxide in the upper troposphere over the Asian monsoon (Li et al., 2005a; Filipiak et al., 2005) and also over the North American summer monsoon (Li et al., 2005b).

3 Results

Fig.1 show the vertical profiles of aerosol Scattering Ratios (SR) measured at Naqu during 6–26 August 2011, along with the daily mean profiles of temperature. The measurements display relatively high aerosol extinction coefficients in the UTLS, which are 4-9 factors higher than those at altitudes below and close to (even higher than, such as on 6 and 12 August) molecular scattering coefficients at the same altitude. Compared with SR profiles of Nabro volcanic aerosol from MPLNET, EARLINET, NDACC and Hefei stations during June and July (Sawamura et al., 2013), the maximum SR of aerosol layers in UTLS over the Tibetan Plateau are

similar to that over Universitat Politècnica de Catalunya, Barcelona, Spain (41.39 °N, 2.11 °E) as one of EARLINET stations but larger than the other observations. Table 1 listed some statistical parameters of aerosol layer over Tibet and Shanghai (31.23 °N, 121.53 °E) for the same period. The highest aerosol extinction coefficients in the UTLS over the Tibetan Plateau generally located at 18-19 km altitudes, which are 1-2 km higher than the tropopause. Tropopause temperatures ranged from -70 ℃ to -80 ℃, and the height of the tropopause varied from 80 hPa to 100 hPa (from 17 km to 18 km), during the observational period. Moreover, such relatively high aerosol extinction coefficients could extend over broad layers, ranging approximately 3-4 km.

The CALIOP aerosol extinction coefficients are available over UTLS for 12, 13, 18 and 20 August. Fig.2 compares the average extinction coefficient profile of MPL with that of CALIOP and shows a good agreement between the two instruments in both aerosol layers altitude and the value of extinction coefficient. In particularly，the MPL profiles show less standard errors at each vertical resolution altitude possibly due to the good signal-to-noise ratio of MPL observed at the high altitude of the lidar station and clear atmospheric environment over the Tibetan Plateau.

According to the period of occurrence of aerosol layers in UTLS, the continuous lidar observation can be split into two stages: 6 to 12 (S1) and 22 to 26 (S2) August 2011 for the continuous maintenance stages of aerosol layer. Between the two stages, the existence of low clouds decayed the lidar signal to the extent that no available aerosol layer observed in UTLS. Additionally, some cases with cirrus in upper troposphere might increase the retrieval error of extinction coefficient of above aerosol layer, which are also removed from the dataset. Fig.3. shows the daily variation in plateau monsoon index (PMI) and the seven-day averaged PMI time series from 1 July to 31 August 2011, with an overlap of cirrus occurrence (He et al. 2013) and aerosol optical depth (AOD) in UTLS. PMI is an indicator of the daily mean intensity of the Tibetan Plateau monsoon. A larger PMI value indicates stronger monsoon in summer, which can be determined as follows (Tang et al. 1984):

$$PMI=H_1+H_2+H_3+H_4-4H_0 \quad (2)$$

where H is the daily deviation from the monthly mean geo-potential height at 600 hPa.

The subscript numbers 0 to 4 indicate the location of the Center (90 °E, 32.5 °N), West (80 °E, 32.5 °N), South (90 °E, 25 °N), East (100 °E, 32.5 °N) and North (90 °E, 40 °N) of the Plateau, respectively.

Many researchers have adopted the PMI to analyze the Tibetan Plateau monsoon variation. It is concluded that the index can reasonably describe the main characteristics of the Tibetan Plateau monsoon (e.g., Bai et al. 2001; Bai et al. 2005; Xun et al. 2011). These two stages might be caused by the different circulation systems due to an apparent time interval of about 10 days with PMI undergoing a substantial oscillation. During the first stage (from 6 to 12 August 2011), when the AOD decreased from 6 to 7 August and increased from 8 to 12 August, the values of PMI experienced an increasing trend from -20 on 6 August to 63 on 12 August. The values sharply decreased to below -40 in the second stage with the low and continuous decreasing AOD over UTLS from 22 to 26 August 2011. Two obvious features can be found in the temporal variation of AOD: (i) AOD showed a decreasing trend companied by decreasing PMI during the campaign period, indicating that the aerosol layers wore off gradually with the reducing intensity of the Asian monsoon over the Tibetan Plateau at the end of August. Bourassa et al. (2012) found that the strong Asian monsoon anticyclone, which existed from June through September over Asia and the Middle East, where the Nabro volcanic aerosol was observed with OSIRIS, and the enhanced aerosol dispersed and quickly circulated throughout the Northern Hemisphere at the end of August, when the Asian monsoon anticyclone began to decay. And (ii) when the intensity of the Tibetan Plateau monsoon circulation subsided to PMI less than 0, the AOD in UTLS kept persistent decline regardless of the variation trend of PMI, indicating that confinement of the air in the lower stratosphere induced by Asian monsoon anticyclone were destroyed to benefit the enhanced aerosol dispersing to the whole Northern Hemisphere.

In these cases, there were interesting temporal change in maximum extinction coefficients of the aerosol layer and the tropopause temperatures, as shown in Fig.4. The maximum extinction coefficients appear to be anti-correlated with the tropopause temperatures. The aerosol extinction coefficient usually increases with decreasing

tropopause temperature along the time series. The maximum extinction coefficient of these cases is 12.0 m^{-1} on 12 August, when the tropopause temperature is -76.0 ℃, being the lowest compared with the other cases. The minimum extinction coefficient of these cases is 4.4 m^{-1} on 26 August, corresponding to the highest tropopause temperature of -72.3 ℃.

There are two possible ways for the decreasing tropopause temperatures to affect the enhancement of high aerosol extinction. One way is the low temperatures due to adiabatic cooling of ascending air parcels induced by deep convective activities, which result in the direct transportation of natural and/or anthropogenic emissions from the troposphere over the Tibetan Plateau. The decreasing temperature at the tropopause is generally associated with the enhancement in deep convective activities over the Tibetan Plateau. The low OLR has been treated as an indicator of the organized deep convective activity in the troposphere (Fujiwara et al., 2009). Fig.5 compares nighttime mean maximum aerosol extinction coefficients in UTLS with the OLR convection proxy over the Tibetan Plateau in August 2011. The enhancement of aerosols near the tropopause appears to be well correlated with the changes in OLR(r^2 = 0.77) without evidence of substantial time lags. Between the two stages, the existence of low clouds in those days might obstruct significantly adiabatic cooling of ascending air parcels and vertical transportation of aerosols in the lower troposphere, resulting in different variation of aerosol layer with intensity of deep convective activity in the two continuous maintenance stages of aerosol layer. The relationships of the aerosol extinction coefficient and OLR in two continuous stages are also shown in Fig. 5 with correlation coefficient of 0.78 and 0.86 for S1 and S2, respectively, suggesting the possibility that the tropopause aerosol enhancement associates with the upward transport of aerosols in deep convective systems over the Tibetan Plateau. The overshooting deep convection could directly influence the aerosol concentration at this level. Using daily NCEP data and monthly SAGE data, Cong et al. (2001) calculated the inter annual change of the aerosol and ozone in 100 hPa, and they proposed that the atmospheric masses passing over the tropopause over the Tibet Plateau and its neighboring areas might possibly carry the aerosol particles of middle

or lower troposphere into the vicinity of the tropopause and result in an increase of the aerosol loading near the tropopause. Yin et al. (2012) used a cloud resolving model coupled with a spectral bin microphysical scheme to investigate the effects of deep convection on the concentration and size distribution of aerosol particles within the upper troposphere, and found that aerosols originating from the boundary layer can be more efficiently transported upward, as compared to those from the mid-troposphere, due to significantly increased vertical velocity through the reinforced homogeneous freezing of droplets. Bourassa et al. (2012) also found a large stratospheric optical depth enhancement after the Nabro eruption over the Tibetan Plateau located on the eastern side of the Asiatic monsoon circulation, where vertical transport to stratospheric altitudes is particularly effective (Park et al., 2007).

The other way for the decreasing tropopause temperatures to affect the enhancement of high aerosol extinction is the enlargement of pre-existing and/or vertically transported aqueous solution droplets induced by adiabatic cooling and hydration of the air associated with deep convection. It has been verified that deep convection over the Tibetan Plateau is likely to be a primary pathway for water vapor from the maritime boundary layer (e.g., Indian Ocean, South China Sea). Dessler and Sherwood (2004) have also suggested that convective transport plays a key role for the accumulation of water vapor near the tropopause, resulting in an increase of H_2O mixing ratio by more than 5 ppmv near the tropopause (Gettelman et al., 2002; Park et al., 2004; Fu et al., 2006). But Tobo et al. (2007) used a growth model to calculate the possible growth under given atmospheric conditions assuming the existence of liquid solutions at equilibrium with respect to H_2O, H_2SO_4 and HNO_3, and found that aerosol growth is sensitive to H_2O mixing ratios. According to the calculated growth curves of liquid solutions as a function of temperature and water vapor, the high H_2O mixing ratios (more than 5 ppmv) are indispensable condition for producing high concentrations of fine particles near the tropopause. In fact, the H_2O mixing ratios near the tropopause and aerosol layer from Vaisala RS92 radiosondes released in 6, 8 11 and 23 August 2011 are not more than 2 ppmv, obviously less than the previous observations, as shown in Fig. 6. In consequence, the effects of gas-to-particle

conversion from liquid solutions would likely be secondary to the enhancement of high tropopause aerosol extinction in these cases.

The continuous variation of water vapor distribution observed by satellite, despite lower vertical resolution, might also be used to investigate the contribution of liquid solutions conversion to the enhancement of high tropopause aerosol extinction. Fig.7 shows the time series of water vapor profile derived from MLS, tropopause level from sounder temperature profiles, and the altitude of daily mean maximum aerosol extinction coefficients in this region. It can be clearly seen that almost all the abundant water vapor transported by deep convective systems are concentrated below 120 hPa altitude (about 15 km). Meanwhile, the temporal correlation of extinction coefficients in aerosol layer with water vapor from day to day is weak with correlation coefficient of 0.36, suggesting that it is impossible that the enhanced tropopause aerosol is due to the condensation of water vapor.

4 Conclusion

In this study, we observed significantly increased aerosol extinction coefficients in UTLS over the Tibetan Plateau by continuous measurements with MPL during summer 2011. The retrieval of MPL showed a good agreement with CALIOP. The maximum SR of aerosol layers, up to 4-9, in the UTLS generally located in 18–19 km m.s.l., 1–2 km higher than the tropopause, with broad layer depth ranging approximately 3–4 km.

Even though the aerosol layers in UTLS wore off gradually with the reducing intensity of the Asian monsoon over the Tibetan Plateau at the end of August, the variation of maximum extinction coefficient of aerosol layers were found to be connected to the local OLR convection proxy. In addition to the eruption of Nabro volcano, appearance of deep transport from the most intense convection is considered to be important factors to explain the enhancement of tropopause aerosols observed in summer over the Tibetan Plateau. Deficiency in water vapor in UTLS indicates that the effects of gas-to-particle conversion from liquid solutions would likely be secondary to the enhancement of high tropopause aerosol extinction in these cases.

It is must be noted that our interpretations are based on a short time observation. It is difficult to conclude that either one of the two processes is dominant due to lack of observations for trace gases. If further observations with more frequent soundings of water vapor and trace gases can be performed to investigate a correlation of high aerosol extinction with ambient temperatures, water vapor, trace gases, liquid solutions and transport processes, the result will be helpful in validating origination and mechanism of the enhanced aerosol extinction in UTLS.

Acknowledgements. This study was supported by Special Funds for Meteorological Research in the Public Interest (Grant Numbers: GYHY201106023, GYHY201006047), the National Natural Science Foundation of China (NSFC, Grant Numbers: 40705013, 40975012 and41175020), the Shanghai Science and Technology Committee Research Special Funds (Grant Number: 10JC1401600). We thank all TOAR team members and the staff from the Tibet Meteorological Service for assisting our experiment work. The authors gratefully acknowledge the NOAA/OAR/ESRL PSD, Boulder, Colorado, USA, for providing the interpolated OLR data on their web site http://www.cdc.noaa.gov/.

References

Bai, H. Z., Xie, J. N., and Li, D. L.: The principal feature of Qinghai-Xizang Plateau monsoon variation in 40 years, Plateau Meteor., 20, 22–27, 2001.

Bai, H. Z., Ma, Z. F., and Dong, W. J.: Relationship between Qinghai-Xizang Plateau region monsoon features and abnormal climate in china, Plateau Meteor., 16, 484–491, 2005.

Bourassa, A., Robock, A., Randel, W., Deshler, T., Rieger, L., Lloyd, N., Llewellyn, E., and Degenstein, D.: Large Volcanic Aerosol Load in the Stratosphere Linked to Asian Monsoon Transport, Science, 337, doi:10.1126/science.1219371, 2012

Borrmann, S., Solomon, S., Avallone, L., Toohey, D., and Baumgardner, D.: On the occurrence of ClO in cirrus clouds and volcanic aerosol in the t ropopause region, Geophys. Res. Lett., 24(16), 2011- 2014, 1997.

Campbell, J. R., Hlavka, D. L., Welton, E. J., Flynn, C. J., Turner, D. D., Spinhirne, J. D., Scott, V. S., and Hwange, I. H.: Full-time, eye-safe cloud and aerosol lidar observation at Atmospheric Radiation Measurement program sites: Instruments and data processing, J. Atmos. Oceanic Technol., 19, 431 – 442, doi:10.1175/1520-0426(2002)019<0431:FTESCA>2.0.CO;2. , 2002.

Clarisse, L., Coheur, P. F., Theys, N., Hurtmans, D., and Clerbaux, C.: The 2011 Nabro eruption, a SO2 plume height analysis using IASI measurements, Atmos. Chem. Phys. Discuss., 13, 31161-31196, doi:10.5194/acpd-13-31161-2013, 2013.

Cong, C. H., Li, W. L., and Zhou, X. J.: Atmospheric mass exchange between the troposphere stratosphere over the Tibetan Plateau and its neighboring regions, Science Bulletin, 46(22), 1914-1918, 2001.

Dessler, A. E. and Sherwood, S. C.: Effect of convection on the summertime extra tropical lower stratosphere, J. Geophys. Res., 109, D23301, doi:10.1029/2004JD005209, 2004.

Dethof, A., O'Neill, A., Slingo, J. M., and Smit, H. G. J.: A mechanism for moistening the lower stratosphere involving the Asian summer monsoon, Q. J. R. Meteorol. Soc., 125, 1079– 1106, 1999.

Fernald, F. G.: Analysis of atmospheric lidar observations: Some comments, Appl. Opt., 23(5), 652– 653, 1984.

Filipiak, M. J., Harwood, R. S., Jiang, J. H., Li, Q., Livesey, N. J., Manney, G. L., Read, W. G., Schwartz, M. J.,

Waters, J. W., and Wu, D. L.: Carbon monoxide measured by the EOS Microwave Limb Sounder on Aura: First results, Geophys. Res. Lett., 32, L14825, doi:10.1029/2005GL022765, 2005.

Fu, R., Hu, Y., Wright, J. S., Jiang, J. H., Dickinson, R. E., Chen, M., Filipiak, M., Read, W. G., Waters, J. W., and Wu, D.: Short circuit of water vapor and polluted air to the global stratosphere by convective transport over the Tibetan Plateau, Proc. Natl. Acad. Sci. USA, 103,5664–5669, 2006.

Fujiwara, M., Iwasaki, S., Shimizu, A., Inai, Y., Shiotani, M., Hasebe, F., Matsui, I., Sugimoto, N., Okamoto, H., Nishi, N., Hamada, A., Sakazaki, T., and Yoneyama, K.: Cirrus observations in the tropical tropopause layer over the western Pacific, J. Geophys. Res., 114, D09304, doi:10.1029/2008JD011040, 2009.

Gettelman, A., Salby, M. L., and Sassi, F.: Distribution and influence of convection in the tropical tropopause region, J. Geophys. Res., 107(D10), 4080, doi:10.1029/2001JD001048, 2002.

Hanson, D. R., Ravishankara, A. R., Solomon, S.: Heterogeneous react ions in sulfuric acid aerosols: A framework for model calculations, J. Geophys. Res., 99(D2), 3615- 3629, 1994.

He, Q., C., Li, J., Ma, H., Wang, G., Shi, Z., Liang, Q., Luan, F., Geng, and X., Zhou: The properties and formation of cirrus clouds over the Tibetan Plateau based on summertime lidar measurements. J. Atmos. Sci. doi:10.1175/JAS-D-12-0171.1, 70, 901-915, 2013.

Highwood, E. J. and Hoskins, B. J.: The tropical tropopause, Q. J. R. Meterol. Soc., 124, 1579– 1604 ,1998.

Hoskins, B. J. and Rodwell, M. J.: A model of the Asian summer monsoon. Part I: The global scale, J. Atmos. Sci., 52, 1329– 1340, 1995.

Jackson, D. R., Driscoll, S. J., Highwood, E. J., Harries, J. E., and Russell, J. M.: Troposphere to stratosphere transport at low latitudes as studied using HALOE observations of water vapour 1992–1997, Q. J. R. Meteorol. Soc., 124, 169– 192, 1998.

Keim, E. R., Fahey, D. W., Delnegro, L. A., Woodbridge, E. L., Gao, R. S., Wennberg, P. O., Cohen, R. C., Stimpfle, R. M., Kelly, K. K., Hintsa, E. J., Wilson, J. C., Jonsson, H. H., Dye, J. E., Baumgardner, D., Kaw, S. R., Salawitch, R. J., Proffitt, M. H., Loewenstein, M., Podolske, J. R., and Chan, K. R.: Observations of large reductions in the NO/NOy ratio near the mid-latitude tropopause and the role of heterogeneous chemistry, Geophys. Res. Lett., 23, 3223-3226, 1996.

Kim, Y. S., Shibata, T., Iwasaka, Y., Shj, G., Zhou, X., Tamuraa, K., and Ohashi, T.: Enhancement of Aerosols near The Cold Tropopause in Summer over Tibetan Plateau: Lidar and Balloon-borne measurements in1999 at Lhasa, Tibet, China, in: Lidar Remote Sensing for Industry and Environment Monitoring III, edited by: Singh U. N., Itabe, T., and Liu, Z., Proceedings of SPIE, Hangzhou, China , 4893, 496-503, 2003.

Li, Q., Jiang, J., Wu, D., Read, W., Livesey, N., Waters, J., Zhang, Y., Wang, B., Filipiak, M., Davis, C., Turquety, S., and Wu, S.: Convective outflow of South Asian pollution: A global CTM simulation compared with EOS MLS observations, Geophys. Res. Lett., 32, L14826, doi:10.1029/2005GL022762, 2005a

Li, Q., Jacob, D., Park, R., Wang, Y., Heald, C., Hudman, R., Yantosca, R., Martin, R., and Evans, M.: North American pollution outflow and the trapping of convectively lifted pollution by upper-level anticyclone, J. Geophys. Res., 110, D10301 doi:10.1029/2004JD005039, 2005b.

Li, W. L. and Yu, S. M.: The characteristics of aerosol spatial and temporal distribution, radiation forcing and climate effect by numerical simulation over the Tibetan Plateau, Sci. in China (Series D), 31(Supp.), 300-307, 2001.

Liebmann, B. and Smith, C. A.: Description of a complete (interpolated) outgoing longwave radiation dataset, Bull. Am. Meteorol. Soc., 77, 1275–1277, 1996.

Miloshevich, L. M., Vömel, H., Whiteman, D. N., Lesht, B. M., Schmidlin, F. J., and Russo, F.: Absolute accuracy of water vapor measurements from six operational radiosonde types launched during AWEX-G and implications for AIRS validation, J. Geophys. Res., 111, D09S10, doi: 10.1029/2005JD006083, 2006.

Miloshevich, L., Vömel, H., Whiteman, D. N., and Leblanc, T.: Accuracy assessment and correction of Vaisala RS92 radiosonde water vapor measurements, J. Geophys. Res., 114(D11), doi: 10.1029/2008JD011565, 2009.

Müller, D., Ansmann, A., Mattis, I., Tesche, M., Wandinger, U., Althausen, D., and Pisani, G.: Aerosol-type-dependent lidar ratios observed with Raman lidar, J. Geophys. Res., 112, D16202, doi:10.1029/2006JD008292, 2007.

NASA: U.S. Standard Atmosphere Supplements, U.S. Govt. Print. Off., Washington, D.C.,1976.

Park, M., Randel, W. J., Gettelman, A., Massie, S. T., and Jiang, J. H.: Transport above the Asian summer monsoon anticyclone inferred from Aura Microwave Limb Sounder tracers, J. Geophys. Res., 112, D16309, doi:10.1029/2006JD008294, 2007.

Park, M., Randel, W. J., Kinnison, D. E., Garcia, R. R., and Choi, W.: Seasonal variation of methane, water vapor, and nitrogen oxides near the tropopause: Satellite observations and model simulations, J. Geophys. Res., 109, D03302, doi:10.1029/2003JD003706, 2004.

Rosenlof, K. H., Tuck, A. F., Kelly, K. K., Russell III, J. M., and McCormick, M. P.: Hemispheric asymmetries in water vapor and inferences about transport in the lower stratosphere, J. Geophys. Res., 102, 13,213– 13,234, 1997.

Sawamura, P., Vernier, J. P., Barnes, J. E., Berkoff, T. A., Welton, E. J., Arboledas, L. A., Guzmàn, F. N., Pappalardo, G., Mona, L., Madonna, F., Lange, D., Sicard, M., Beekmann, S. G., Payen, G., Wang, Z., Hu, S., Tripathi, S. N., Jabonero, C. C., and Hoff, R. M.: Stratospheric AOD after the 2011 eruption of Nabro volcano measured by lidars over the Northern Hemisphere, Environ. Res. Lett., 7(3), doi:10.1088/1748-9326/7/3/034013, 2013

Solomon, S.: Stratospheric ozone depletion: a review of concept and history, Rev. Geophys., 37, 275-316, 1999.

Solomon, S., Borrmann, S., Garcia, R. R., Portmann, R., Thomason, L., Poole, L. R., Winker, D., and McCormick, M. P.: Heterogeneous chlorine chemistry in the tropopause region, J. Geophys. Res., 102(D17), 21411- 21429, 1997.

Tang, M. C., Liang, J., Shao, M. J., and Shi, G.: Preliminary analysis on the yearly variation of Tibetan Plateau monsoon, Plateau Meteor., 3, 76–82, 1984.

Tobo, Y., Zhang, D., Iwasaka, Y., Shi, G., Kim, Y., Ohashi, T., Tamura, K., and Zhang, D.: Balloon-borne observations of high aerosol concentrations near the summertime tropopause over the Tibetan Plateau, Atmos. Res., 84, 233-241, 2007.

Tukiainen, S., Kujanpää, J., Bingen, C., Robert, C., Tétard, C., and Dekemper, E.: Nabro volcano aerosol in the stratosphere over Georgia, South Caucasus from ground based spectrometry of twilight sky brightness, Atmos. Meas. Tech., 6, 2563-2576,doi:10.5194/amt-6-2563-2013, 2013

Uchino, O., Sakai, T., Nagai, T., Nakamae, K., Morino, I., Arai, K., Okumura, H., Takubo, S., Kawasaki, T., Mano, Y., Matsunaga, T., and Yokota, T.: On recent(2008–2012) stratospheric aerosols observed by lidar over Japan, Atmos. Chem. Phys., 12, 11975-11984, doi:10.5194/acp-12-11975-2012, 2012.

Vömel, H. H., Selkirk, L., Miloshevich, J., Valverde-Canossa, J., Valdes, J., and Diaz, J.: Radiation Dry Bias of the Vaisala RS92 Humidity Sensor, J. Atmos. Ocean. Tech., 24, 953–963, 2007.

Währn, J., Oyj, V., Rekikoski, I., Jauhiainen, H., and Hirvensalo, J.: New Vaisala Radiosonde RS92: Testing and Results from the Field, Eighth Symposium on Integrated Observing and Assimilation Systems for Atmosphere, Oceans, and Land Surface, Seattle, USA, 13 January 2004, 2004.

Waters, J. W., Froidevaux, L., Harwood, R. S., Jarnot, R. F., Pickett, H. M., Read, W. G., Siegel, P. H., Cofield, R. E., Filipiak, M. J., Flower, D. A., Holden, J. R., Lau, G. K., Livesey, N. J., Manney, G. L., Pumphrey, H. C., Santee, M. L., Wu, D. L., Cuddy, D. T., Lay, R. R., Loo, M. S., Perun, V. S., Schwartz, M. J., Stek, P. C., Thurstans, R. P., Boyles, M. A., Chandra, K. M., Chavez, M. C., Chen, G. S., Chudasama, B. V., Dodge, R., Fuller, R. A., Girard, M. A., Jiang, J. H., Jiang, Y., Knosp, B. W., LaBelle, R. C., Lam, J. C., Lee, K. A., Miller, D.,

Oswald, J. E., Patel, N. C., Pukala, D. M., Quintero, O., Scaff, D. M., Van Snyder, W., Tope, M. C., Wagner, P. A., and Walch, M. J.: The Earth Observing System microwave limb sounder (EOS MLS) on the Aura satellite, IEEE T. Geosci. Remote, 44, 1075– 1092, 2006.

Winker, D. M., Pelon, J., and McCormick, M. P.: The CALIPSO mission: Space borne lidar for observation of aerosols and clouds, Proc. SPIE, 4893, 1–11, 2003.

Wu, P.M., Okada, K., Tanaka, T., Sasaki, T., Nagai, T., Fujimoto, T., and Uchino, O.: Balloon observation of stratospheric aerosols over Tsukuba, Japan Two years after the Pinatubo volcanic eruption, J. Meteor. Soc. Jpn., 72, 475–480, 1994.

Xun, X. Y., Hu, Z. Y., Cui, G. F., He, H. G., Sun, J., Hao, L., and Gu, L. L.: Change of monsoon in Qinghai-Xizang Plateau and its correlation with summer precipitation of Ordos Plateau, J. Arid Land Resour. Environ., 25 (4), 79–83, 2011.

Yan, X. L.: The observation and study on the upper troposphere and lower stratosphere water vapor and ozone over Tibetan Plateau and its adjoint regions, master's thesis, Beijing: Chinese Academy of Meteorological Sciences, 2012.

Yanai, M., Li, C., and Song, Z.: Seasonal heating of the Tibetan Plateau and its effects on the evolution of the Asian summer monsoon, J. Meteorol. Sci. Jpn., 70, 319– 351, 1992.

Yin, Y., Chen, Q., Jin, L., Chen, B., Zhu, S., and Zhang, X.: The effects of deep convection on the concentration and size distribution of aerosol particles within the upper troposphere: A case study, J. Geophys. Res., 117, D22202, doi:10.1029/2012JD017827, 2012.

Table 1 Statistical parameters of aerosol layer over Tibet and Shanghai. Maximum extinction coefficient (EC_{max}), Averaged extinction coefficient (EC_{ave}), aerosol layer depth(ALD), aerosol layer height over sea level and aerosol optical depth (AOD) of the aerosol layer from 20:00 to 06:00 local standard time (LST). The numbers in parenthesis correspond to the standard deviations.

	$EC_{max}(km^{-1})$	$EC_{ave}(km^{-1})$	ALD(km)	ALH(km)	AOD
Tibet	0.007	0.002(0.002)	3.604(1.626)	18.492(0.248)	0.016(0.002)
Shanghai	0.010	0.006(0.003)	4.380(0.764)	16.860(0.839)	0.027(0.006)

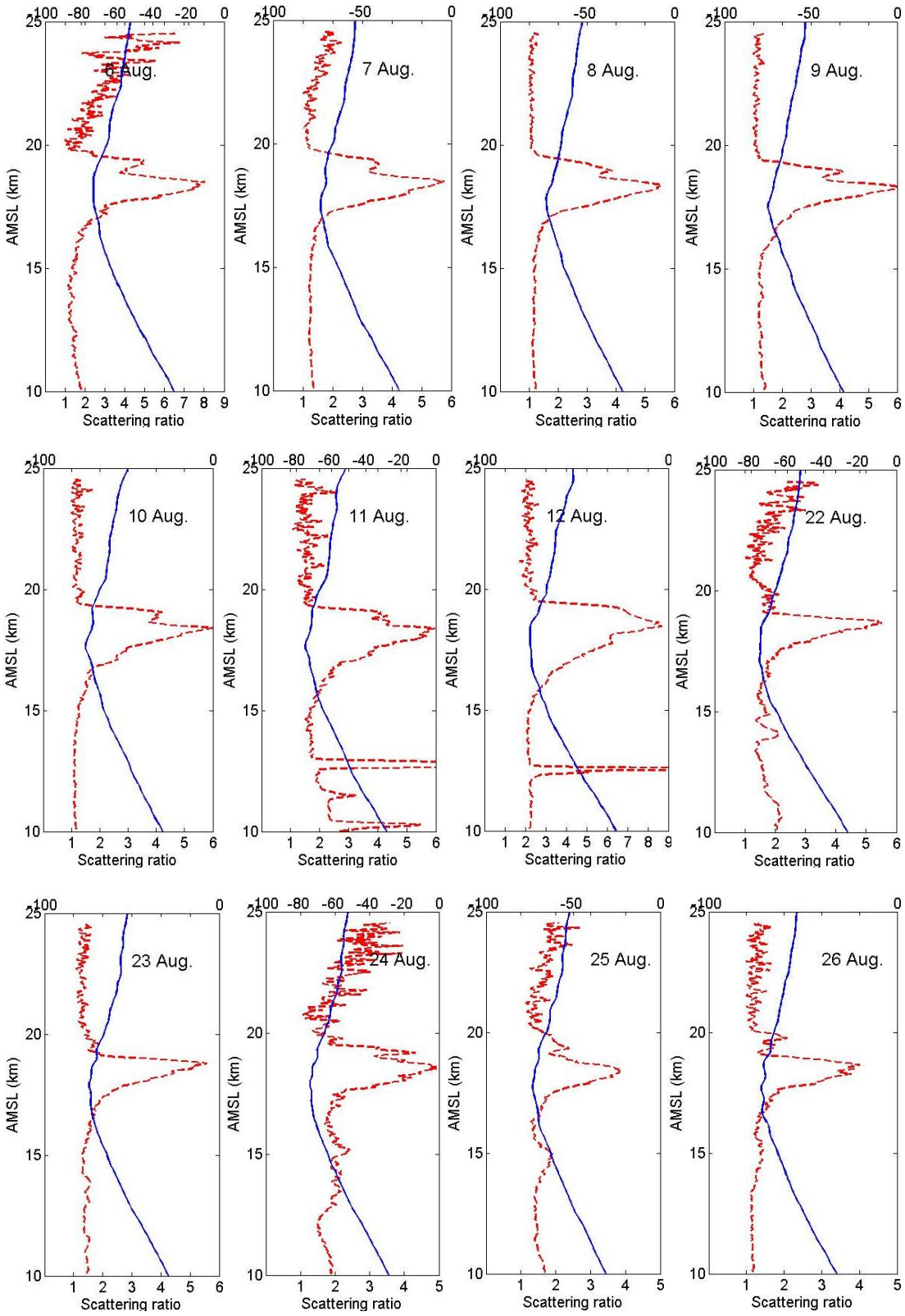

Fig. 1. The nighttime mean aerosol scattering ratio profiles (dashed line) from MPL. The daily mean profiles of temperature (solid line ℃) from the two radiosondes each day are overlaid to indicate the altitude of the tropopause (~18 km m.s.l.).

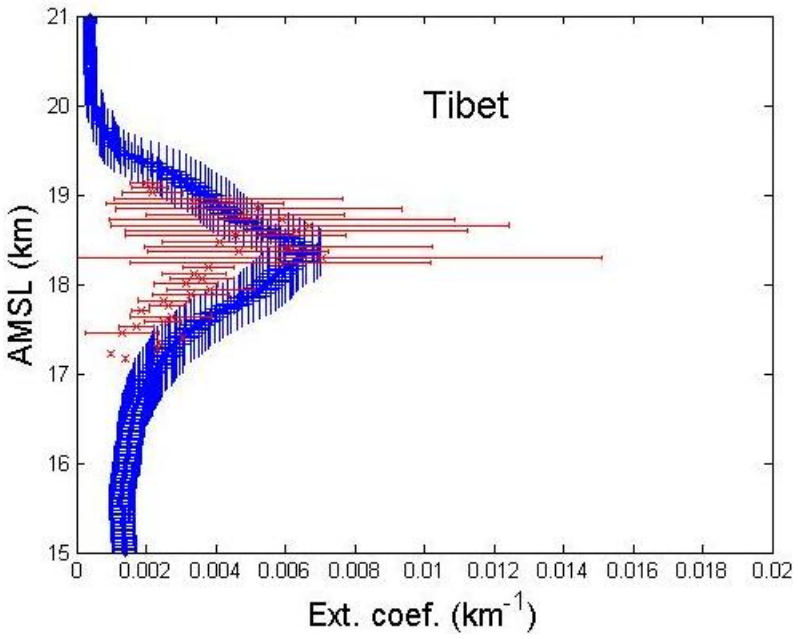

Fig.2. The average extinction coefficient profile of MPL (blue solid line)and the average extinction coefficient at each layer from CALIOP (red stars) during the whole observation period. The standard errors are marked as the error bar.

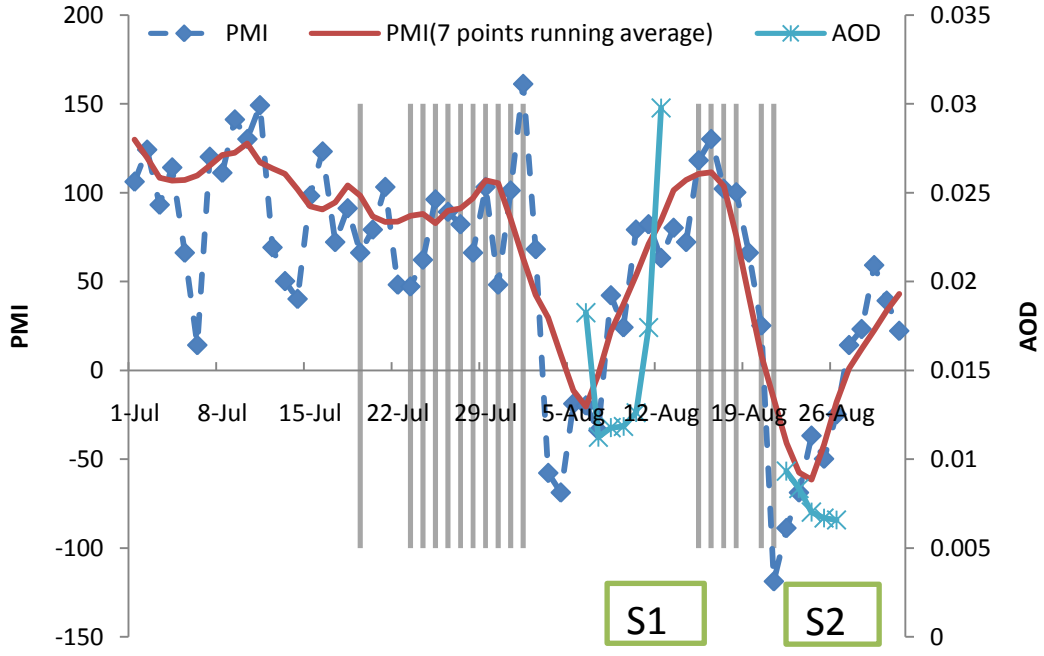

Fig. 3. Daily variation of PMI and the 7-day-averaged PMI time series from 1 Jul to 31 Aug 2011and AOD in UTLS retrieved from MPL over the Tibetan Plateau. The days with cirrus occurrence are shaded (He et al. 2013).

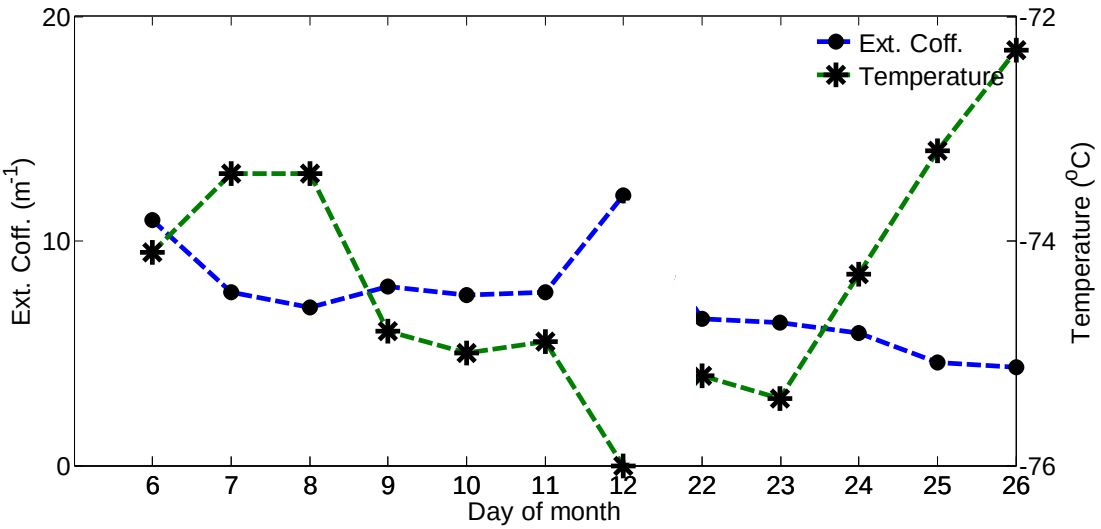

Fig. 4. The time series of maximum extinction coefficient in the aerosol layers and temperature at the tropopause over the Tibetan Plateau day-on-day in August 2011.

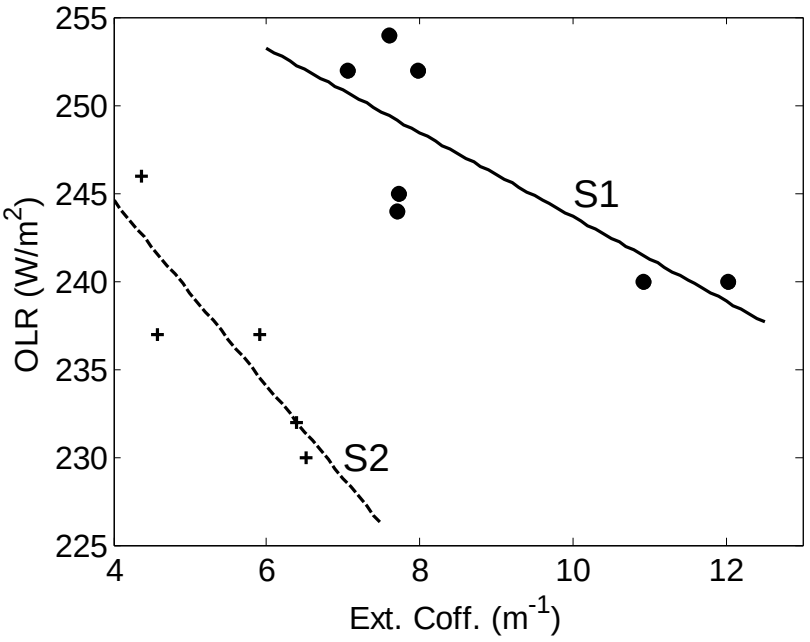

Fig. 5. Nighttime mean maximum extinction coefficient in the aerosol layer vs. OLR. The dots represent the data for 6–12 August (S1) and the pluses for 22–26 August 2011 (S2).

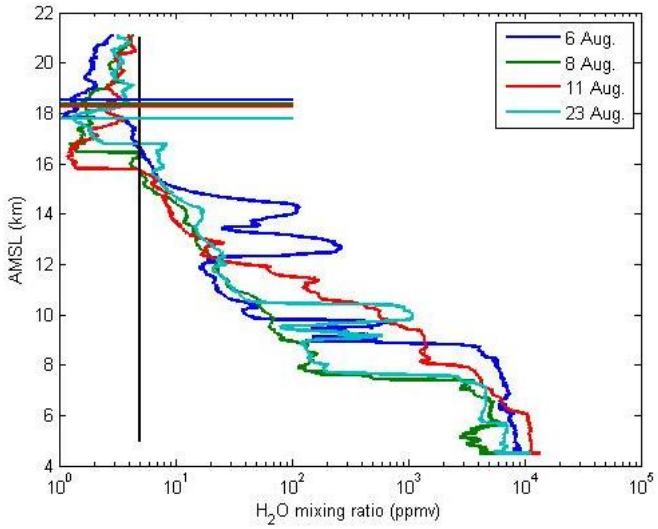

Fig. 6. Vertical profiles of water vapor from Vaisala RS92 radiosondes released in 6, 8, 11 and 23 August 2011, respectively. The black line along *y* axis represents the 5 ppmv of water vapor mixing ratio. The color lines along *x* axis are the altitudes with the maximum extinction coefficient of aerosol layers for each day.

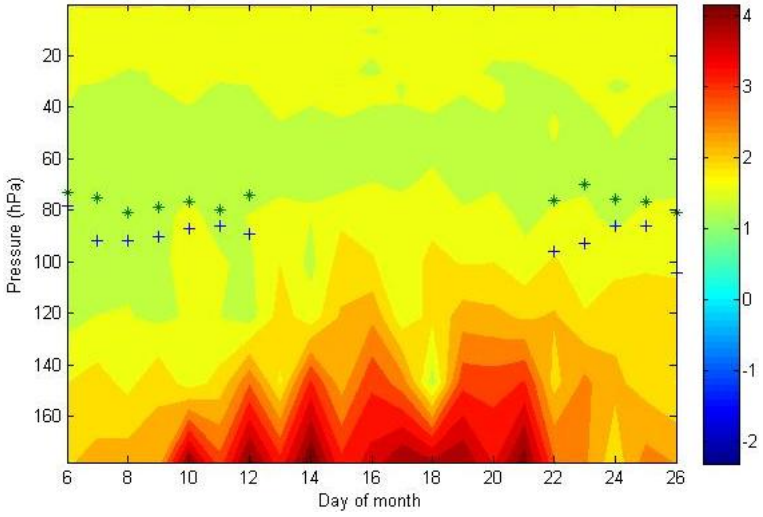

Fig. 7. Altitude-time distributions of MLS water vapor (ppmv, color bar in natural logarithm) from 6 to 26 August 2011. Stars indicate the layer with nighttime mean maximum extinction coefficient and pluses stand for the tropopause level of each day, respectively.